Applied Physics Letters

# Tunable spectral squeezers based on monolithically integrated diamond Raman resonators

Cite as: Appl. Phys. Lett. **120**, 151101 (2022); https://doi.org/10.1063/5.0088592
Submitted: 01 March 2022 • Accepted: 01 April 2022 • Published Online: 11 April 2022

E. Granados, G. Stoikos, D. T. Echarri, et al.







AIP Publishing

Applied Physics Letters ARTICLE scitation.org/journal/apl

# Tunable spectral squeezers based on monolithically integrated diamond Raman resonators

Cite as: Appl. Phys. Lett. **120**, 151101 (2022); doi: 10.1063/5.0088592
Submitted: 1 March 2022 · Accepted: 1 April 2022 ·
Published Online: 11 April 2022



E. Granados,[1,a)] G. Stoikos,[1,2] D. T. Echarri,[1,3] K. Chrysalidis,[1] V. N. Fedosseev,[1] C. Granados,[4] V. Leask,[1,5] B. A. Marsh,[1] and R. P. Mildren[6]

## AFFILIATIONS

[1]CERN, 1217 Geneva, Switzerland
[2]National Technical University of Athens, Athens 106 82, Greece
[3]Universidad de Navarra, Tecnun, Manuel Lardizabal 13, 20018 Donostia, Spain
[4]Max-Born-Institut für Nichtlineare Optik und Kurzzeitspektroskopie, 12489 Berlin, Germany
[5]University of Strathclyde, 99 George Street, Glasgow G1 1RD, United Kingdom
[6]MQ Photonics Research Centre, Macquarie University, Sydney, NSW 2109, Australia

[a)]Author to whom correspondence should be addressed: eduardo.granados@cern.ch

## ABSTRACT

We report on the generation and tuning of single-frequency laser light in a monolithic Fabry–Pérot diamond Raman resonator operating in the visible spectral range. The device was capable of squeezing the linewidth of a broad multi-mode nanosecond pump laser ($\Delta\nu_p = 7.2 \pm 0.9$ GHz at $\lambda_p = 450$ nm) to a nearly Fourier-limited single axial mode Stokes pulse ($\Delta\nu_S = 114 \pm 20$ MHz at $\lambda_S = 479$ nm). The tuning was achieved by precise adjustment of the resonator temperature, with a measured frequency-temperature tuning slope of $\partial\nu_0/\partial T \approx -3$ GHz/K, and a temperature dependence of the first-order Raman phonon line of $\partial\nu_R/\partial T \approx +0.23$ GHz/K. The Stokes center frequency was tuned continuously for over 20 GHz (more than twice the free spectral range of the resonator), which, in combination with the broad Ti:Sapphire laser spectral tunability, enables the production of Fourier-limited pulses in the 400–500 nm spectral range. The Stokes center-frequency fluctuations were 52 MHz (RMS) when the temperature of the resonator was actively stabilized. Moreover, the conversion efficiency was up to 30%, yielding an overall power spectral density enhancement of >25× from pump to Stokes pulse.



Fourier-limited nanosecond pulses are important tools for applications exploiting light–atom interactions at high intensity. Beyond the requirement for a specific linewidth, precise tunability plays a crucial role for the spectroscopic study of narrow-band transitions,[1,2] atomic clocks and cooling,[3,4] or photonic quantum technology.[5–8] One key aspect hindering progress is in the complexity and scaling of individually and precisely tuned single-frequency laser sources at distinct wavelengths across the spectrum.

Beyond the problem of generating Fourier-limited pulses, realizing gigahertz-range frequency shifts with high accuracy while maintaining high efficiency and low loss—in particular, using a miniature and scalable device—is challenging because it requires efficient and controllable nonlinear processes. Typical integrated approaches used for this task are based on acousto-optics,[9,10] wave-mixing,[10,11] and electro-optics.[12] Acousto-optic modulators use phonon scattering to control the light center-frequency and can provide shifts in the kHz to few GHz range while being implemented on a silicon chip.[13] Wave-mixing can achieve efficient frequency conversion but requires stringent phase-matching conditions and is difficult to control due to a strong nonlinear dependence on optical power. The electro-optic effect typically produces parasitic side-bands, which requires additional spectral filtering elements to reduce spectral noise.

Alternatively, stimulated Raman scattering (SRS) and stimulated Brillouin scattering (SBS) can lead to the generation of highly coherent photons in a large variety of materials and at varied wavelengths,[14–16] some of which are suitable for integration on photonic chip

platforms.[17–19] Unlike typical inversion lasers, the emissions from stimulated-scattering lasers are not limited to specific wavelength ranges since no real energy levels are required; this provides unique advantages, such as access to unconventional wavelengths and compatibility with other integrated laser sources. In addition, the generation of the single longitudinal mode (SLM) laser light via SRS can directly provide an intrinsically stable single-frequency output without the parasitic effects of spatial hole burning mode competition,[20] although typically requires elaborated feedback loops to stabilize the cavity length.[21–24]

Recently, by embedding the laser resonator in the Raman media, it has been demonstrated that is possible to produce frequency stable output from a Fabry–Pérot (FP) diamond resonator without the need of external mechanical feedback loops to control the cavity length given that the temperature of the crystal is stabilized.[25] Moreover, these resonators can perform complex functions, such as "linewidth squeezing" when pumped by few GHz linewidth multi-mode lasers. Such mechanism, supported by phonon-resonant Raman interactions, directly enhances the power spectral density (PSD) of broadband nanosecond lasers by 50×. Furthermore, by operating in the so-called high Raman gain regime[14,16]—where the gain bandwidth is reduced to that of the pump laser, the constraints in the design of a resonator to support a single axial mode are further relaxed.

In this work, we build upon these recent demonstrations and present a tunable monolithic diamond Raman converter pumped by a frequency-doubled broadband nanosecond Ti:Sapphire laser. We demonstrate that the combination of FP diamond resonators with widely tunable multi-mode pump lasers not only is capable of producing a nearly Fourier-limited single-frequency pulses but also can be precisely tuned with an accuracy better than <52 MHz RMS over the entire spectral range of the pump laser tuning.

The monolithic Fabry–Pérot Raman medium was a synthetic diamond cuboid crystal with dimensions of $6 \times 2 \times 2\,\text{mm}^3$ [free spectral range (FSR) at 479 nm ≈ 9.5 GHz], plane-cut for beam propagation along the ⟨110⟩ axis, and end-faces re-polished with a parallelism better than 0.5 $\mu$m/mm. Thanks to the high Raman gain of diamond at 450 nm, the Fresnel reflectivity of un-coated surfaces ($R_1, R_2 \approx 18\%$) was sufficient to ensure highly efficient operation. A curved retro-reflector (M1) was used for circulating the pump pulse twice through the Raman medium, ensuring high conversion efficiency. The diamond crystal was placed on a copper mount inside a high precision oven (Covesion Ltd), with a temperature stability <10 mK.

The experiments were carried out using the tunable output provided by an intracavity frequency-doubled gain-switched Ti:Sapphire laser operating at 450 nm, similar to the one described in Refs. 14 and 26. Figure 1 shows a schematic diagram of the experimental setup. The Ti:Sapphire laser was pumped by the second harmonic of a Q-switched Nd:YAG laser (Innolas Nanio 532–20-V) producing up to 18 W of 532 nm light at a 10 kHz repetition rate, although only 8 W was used. The resulting pulse length of the Ti:Sapphire was 50 ns long, with a smooth temporal profile of asymmetric Gaussian shape. The second harmonic of the Ti:Sapphire laser was efficiently produced by intracavity frequency-doubling and exhibited a $\text{TEM}_{00}$ Gaussian mode with an $M^2 < 1.3$. The second harmonic was then extracted from the Ti:Sapphire cavity by means of a dichroic mirror (DM1).

With this configuration, the system was capable of producing approximately 1.2 W of average power at 450 nm, with a continuously tunable output ranging from 350 to 470 nm. The output was focused into the diamond crystal by a 150 mm focal length lens, producing a waist of $57 \pm 5\,\mu$m in diameter and a resulting intensity of $0.1\,\text{GW/cm}^2$. The linewidth (FWHM) of the 450 nm light was measured with a wavelength meter LM-007 (CLUSTER LTD Moscow) and was 7.2 ± 0.9 GHz averaged over ∼1000 shots. In order to separate the pump from the Stokes output, a pair of dichroic mirrors (DM2 and DM3) were used, being possible to tune their angle to optimize the transmission of the pump and the reflection of the Stokes wavelength. The resulting tuning range depends both on the tunability of the pump laser as well as the spectral response of the dichroic mirrors in use.

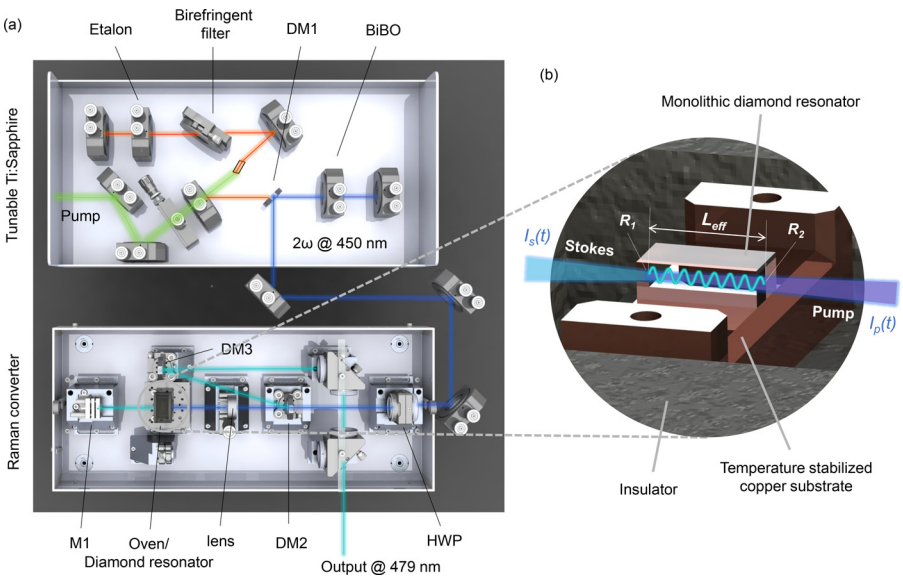


**FIG. 1.** Experimental setup. (a) A widely tunable frequency-doubled gain-switched Ti:Sapphire laser was used for pumping the Raman converter, its polarization control was performed using a half-wave plate (HWP) and a lens to focus it into the diamond resonator. (DM1) Dichroic mirror for separating fundamental and second harmonic beams, (DM2, DM3) Dichroic mirrors for separating pump at 450 nm and Stokes at 479 nm, (M1) curved retro-reflector. (b) Detail of the monolithic diamond resonator mounted on a temperature stabilized copper substrate within the insulated oven. $R_1$ and $R_2$ are the diamond surface reflectivites and $L_{\text{eff}}$ the effective resonator length. $I_p(t)$ and $I_S(t)$ represent the intensity amplitude envelopes in the time domain of the pump and Stoke pulses, respectively.

The theory underlying the complex interplay between pump and Stokes spectral modes has been described in detail in Ref. 25. Here, we only discuss the most important modifications to adapt it to our experimental situation, in particular, regarding the effects of the temperature on the resonating Stokes mode frequency $\nu_0$.

In contrast to previous works, our resulting Stokes frequency was precisely tunable (in the MHz range) using temperature while the pump laser modes were also tuned coarsely (in the multi-GHz domain) using intra-cavity spectral elements. The condition to obtain a spectral "funneling" effect described in Ref. 25, therefore, needs to be modified to

$$\nu_0(T) = \nu_{F(l)} - (\nu_R(T) \pm \Omega l). \quad (1)$$

Here, the term $(\nu_R(T) \pm \Omega l)$ accounts for a phonon that resonantly interacts with the fundamental field mode $\nu_{F(l)}$ and is within the Raman linewidth ($\Delta\nu_R > \Omega l \ \forall l$). $\Omega$ is the pump laser mode spacing. This situation corresponds to the sketch shown in Fig. 2(a) at $T = T_0$. The Raman shift $[\nu_R(T)]$ is temperature-dependent, and the resonating wavelength is determined by the mode closest to the peak of the temperature dependent Raman spectral gain as depicted in Fig. 2(b). Both effects and gain depletion dynamics interplay resulting in a specific Stokes center-frequency. Tuning adiabaticity is ensured by the continuous nature of the parameters involved in the process, with the exception of eventual mode-hops occurring at the edges of the resonator FSR. Meanwhile, the output linewidth is largely determined by the temporal characteristics of the fundamental field and the photon lifetime of the monolithic resonator, both of which are independent of temperature.

The sufficient conditions to ensure a single frequency operation of monolithic diamond resonators were studied in Ref. 25: First, the integrated resonator shall operate in the high Raman gain regime so that the Raman gain spectral width approaches the pump spectral width ($\Delta\nu_R \approx \Delta\nu_P$). Second, the free spectral range (FSR) of the diamond resonator needs to be larger than the pump laser linewidth (FSR $>\Delta\nu_P$). The high Raman gain regime condition is fulfilled here by adjusting the Raman gain to values similar to Ref. 25. In our experiments, the pump intensity was comparatively lower (0.1 GW/cm$^2$ compared to 0.3 GW/cm$^2$), but thanks to the favorable scaling of the Raman gain with shorter pump wavelengths,[27] the resulting gain was equivalent for both cases. The selected diamond had a FSR of 9.5 GHz compared to the 7.2 GHz linewidth of the pump laser ensuring single longitudinal mode operation.

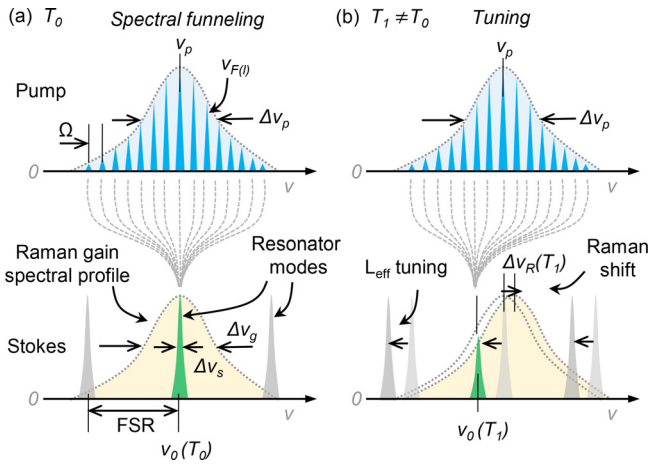


**FIG. 2.** Schematic depiction of (a) spectral funneling effect in monolithic diamond Raman lasers and (b) tuning of the funneling employing temperature.

The diamond converter produced a shifted Stokes output at 479 nm with <114 MHz linewidth at 30% power conversion efficiency (slope efficiency 58%), yielding a maximum peak power spectral density (PSD) enhancement of >25×, as shown in Fig. 3. The PSD normalization was carried out scaling the spectral curves so that their integrals correspond to the measured pulse energies.

The frequency stability results are shown in Fig. 4. Here, the diamond bulk was temperature stabilized with an accuracy <10 mK, and the resulting RMS fluctuation of the output Stokes center frequency was <52 MHz, measured over a period of two hours with a sampling rate of 15 Hz.

The measured peak-to-peak frequency fluctuation was <200 MHz. These fluctuations are assumed to be related to environmental factors, although a likely correlation between pump pulse energy and Stokes center frequency—due to the variable laser heat deposition in the crystal—also could render deviations in the resonator effective length. Likewise, the temperature gradient generated by the laser illumination of an area of only 160 $\mu$m$^2$ could in principle account for some discrepancy between the bulk temperature measurements and the actual diamond temperature at which the Raman interaction takes place. Such deviations, however, are assumed to be negligible due to the power stability of the pump laser (less than 1% RMS power fluctuations) and the high thermal conductivity of the diamond crystal, and so not affecting considerably the tuning slope.

In order to study the temperature dependency, we define "effective length" ($L_{eff}$) as the exact optical path length between

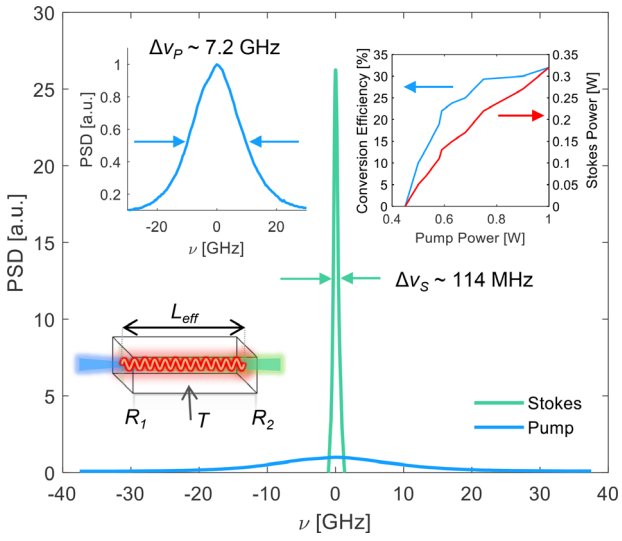


**FIG. 3.** Normalized power spectral density profile of the pump and Stokes pulses at maximum conversion efficiency. (Inset left) Pump pulse linewidth measurement. (Inset right) Slope and conversion efficiency. (Inset down) Sketch of the monolithic Fabry–Pérot diamond resonator, where $R_1$ and $R_2$ are the reflectivities of the parallel end-surfaces, $T$ is the temperature setting, $L_{eff}$ is the effective medium length at $\nu_0$.

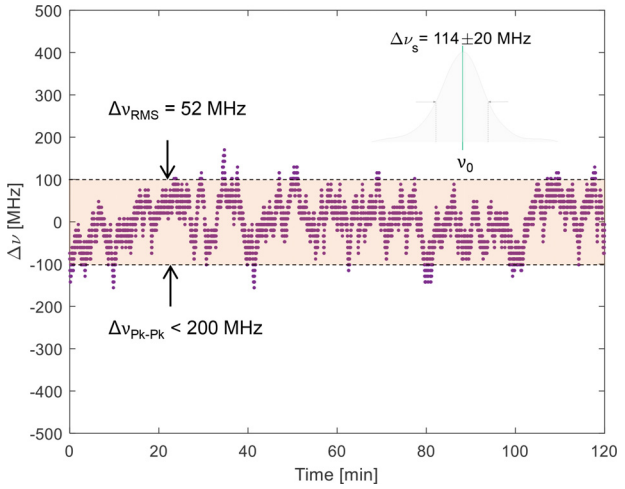


**FIG. 4.** Stokes frequency stability over a period of 2 h under constant temperature. (Inset) average measured Stokes linewidth during the same period.

resonator facets at a particular Stokes wavelength $\lambda_S$, which defines the resonating Stoke longitudinal modes frequencies. For Raman processes, the temperature dependence of the first-order Raman phonon line needs also to be taken into account to predict the output Stokes frequency accurately.

In general, it is possible to calculate separately the effects that produce a shift to the Stokes resonant frequency $\nu_0$. The temperature affects the optical length of the resonator as well as the Raman shift. The effective length or optical path length at the wavelength $\lambda_S$ and at temperature $T_0$ can be defined as

$$L_{\text{eff}}(T_0, \lambda_S) = L(T_0)n(T_0, \lambda_S). \tag{2}$$

The condition for resonance within the diamond resonator is

$$\lambda_S(T_0) = \frac{2}{q}L_{\text{eff}}(T_0, \lambda_S) = \frac{2}{q}L(T_0)n(T_0, \lambda_S), \tag{3}$$

where $q$ is the mode number. Note that all wavelengths used in this mathematical formulation are in vacuum. For small shifts in temperature ($\Delta T$), we can use a perturbation theory approach to estimate the resulting wavelength shift of the Stokes by

$$\lambda_S(T_0 + \Delta T) = \frac{2}{q}\left(L(T_0) + \frac{\partial L}{\partial T}\Delta T\right) \times \left(n(T_0, \lambda_S) + \frac{\partial n}{\partial T}\Delta T + \frac{\partial n}{\partial \lambda}\Delta\lambda_S\right). \tag{4}$$

Here, the term $\partial L/\partial T$ can be expressed in terms of the linear thermal expansion coefficient ($\alpha$ in the following) as $\partial L/\partial T = \alpha L(T_0)$. The shift in wavelength can be directly calculated by $\Delta\lambda_S = \lambda_S(T_0 + \Delta T) - \lambda_S(T_0)$. The terms $\partial n/\partial T$ and $\partial n/\partial\lambda$ correspond to the thermo-optic coefficient at $T_0$ and the chromatic dispersion at $\lambda_S$, respectively. Here, we assume that dispersion terms do not change for small temperature increments $\Delta T$.

Reorganizing Eq. (4) and neglecting second order differential terms, we can obtain an approximate tuning slope of the center Stokes wavelength as a function of temperature. Changing variables from Stokes wavelength $\lambda_S$ to resonating Stokes frequency $\nu_0$, Eq. (4) becomes

$$\frac{\partial \nu_0}{\partial T} = -\frac{c}{\lambda_S}\frac{(1/n)(\partial n/\partial T) + \alpha}{1 - \lambda_S(1/n)(\partial n/\partial\lambda)}. \tag{5}$$

Note that, in general, the thermo-optic coefficient is a function of temperature and, therefore, the tuning slope will have a resulting temperature dependence; here, we take into account only the first-order term. It is apparent from Eq. (5) that in order to obtain an accurate and stable tune of the Stokes wavelength, materials exhibiting low thermo-optic coefficient and low thermal expansion coefficient $\alpha$ will present an advantage. Similarly, highly dispersive materials may further reduce requirements for temperature accuracy when high Stokes frequency stability is pursued.

Using Eq. (5), the expected values for the tuning slope in frequency $(\Delta\nu_0/\Delta T)$ in the range from 300–400 K vary from −2.7 to −3.6 GHz/K as shown in Fig. 5(b). For this estimation, the thermo-optic coefficient was calculated using the model described in Ref. 28, whereas the dispersion was calculated using the two-factor Sellmeier equation for synthetic diamond found in Ref. 29 and the thermal expansion coefficient of $\alpha \sim 1.1 \times 10^{-6}\ \text{K}^{-1}$ found in Ref. 30.

The peak position $\nu_R$ and the linewidth of the first-order Raman mode of diamond at $\sim$1332 $\text{cm}^{-1}$ are also a function of temperature. At a certain temperature $T$, the an-harmonic interactions can effectively change the unperturbed Raman frequency at 0 K. From a Klemens model, which assumes that the zone-center optical modes decay into two acoustical phonons of opposite momentum, the first order Raman line shifts by temperature as follows:[31]

$$\nu_R(T) = -B\left(\frac{2}{e^{\hbar\omega_0/2k_BT} - 1}\right), \tag{6}$$

where the unit-less scaling factor $B$ depends on the details of the diamond dispersion curves.[31] A fit to the experimental data shown in Ref. 31 yields a value of $B = 1.3 \times 10^{12}$. Here, $\hbar\omega_0 = 1332.7\ \text{cm}^{-1}$ is the Raman shift at 0 K. It is worth noting that a negative $\nu_R(T)$ produces a higher Stokes frequency, and so the tuning slope of the Stokes center frequency will have a resulting positive sign. Differentiating Eq. (6), we obtain an analytical expression for the Raman shift tuning slope,

$$\frac{\partial \nu_R}{\partial T} = -B\frac{\hbar\omega_0 e^{(\hbar\omega_0/2k_BT)}}{k_BT^2(e^{(\hbar\omega_0/2k_BT)} - 1)^2}. \tag{7}$$

Using Eq. (7), the theoretical values for $(\partial\nu_R(T)/\partial T)$ in the range from 300–400 K induce a frequency shift in the center Stokes frequency from +0.2 GHz/K to +0.25 GHz/K as shown in Fig. 5(c).

From the calculated slope in Eq. (7), it is clear that for attaining a frequency stability below 100 MHz required for typical high-resolution spectroscopy or quantum applications, the temperature of the diamond resonator needs to be stabilized with an accuracy of at least <40 mK.

The tunability experimental tests were carried out by adjusting the temperature setting of the oven in increments of 10 mK, and the results are shown in Fig. 5(a). The average frequency-temperature tuning slope within a FSR of the resonator was approximately $\partial\nu_0/\partial T \approx -3$ GHz/K, whereas the temperature dependence of the first-order Raman phonon line was about $\partial\nu_R/\partial T \approx +0.23$ GHz/K. This agrees

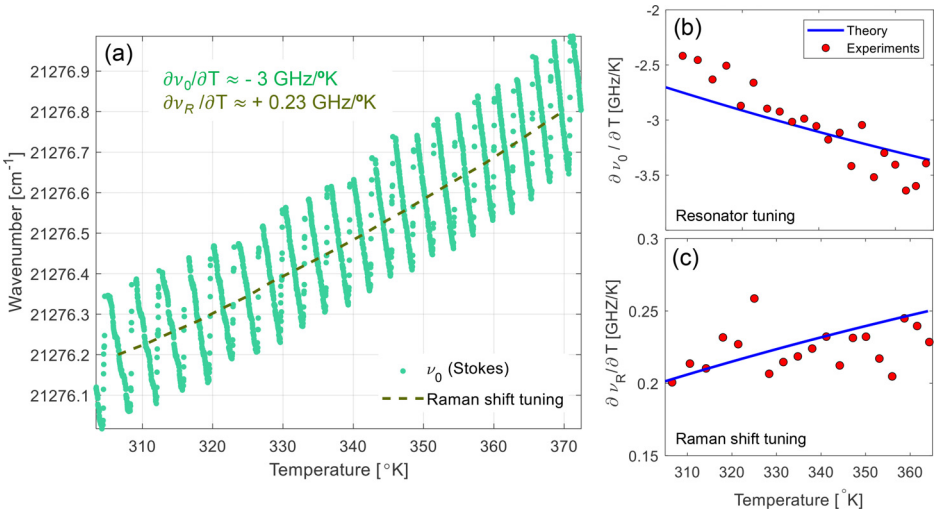


**FIG. 5.** (a) Stokes center frequency ($\nu_0$) as a function of measured diamond surface temperature. Dashed line represents the tuning of the Raman shift as a function of temperature. Measured and calculated tuning slope due to (b) the variation of resonator effective length with temperature and (c) due to the Raman shift variation with temperature.

reasonably with previous calculations resulting from the Klemens model ($\approx +0.2$ to 0.25 GHz/K) and with the temperature dependent effective length calculations ($-2.7$ to $-3.6$ GHz/K) as shown in Figs. 5(b) and 5(c). It can be appreciated that the overall tuning slope is a nonlinear function of temperature due to the temperature dependency of the thermo-optic coefficient.[28] Interestingly, the range where the index of refraction is nonlinear is most severe for temperatures in the range from 200 to 400 K. Below 200 K, $(1/n)\partial n/\partial T$ is nearly zero, whereas for values above 400 K, it asymptotically tends to $7.1 \times 10^{-6}$ $K^{-1}$. Within a small tuning ranges smaller than the FSR, the response was mostly linear, suggesting also that mode-pulling effects were essentially negligible.

The results portray also the possibility of selecting the optimal temperature range for ensuring that the Stokes frequency is at the center of the resonator FSR. This is thanks to the relatively small Raman shift temperature tuning compared to the thermo-optic and thermal expansion effects on the Stokes frequency. Such feature can be then exploited to facilitate pure single frequency operation without spectral side-modes, ensuring maximal output power and PSD simultaneously.

This work demonstrates that an inherently robust and simple monolithic diamond resonator can efficiently transform pulsed broad-band tunable laser radiation into a near-Fourier limited and continuously tunable output with significantly increased power spectral density. Our results show that tunable integrated FP diamond Raman resonators hold great promise for the on-chip generation of high intensity tunable narrow linewidth light across the optical spectrum, with broad ranging spectroscopy and quantum optics applications.

## AUTHOR DECLARATIONS

### Conflict of Interest

The authors have no conflicts to disclose.

## DATA AVAILABILITY

The data that support the findings of this study are available from the corresponding author upon reasonable request.

## REFERENCES

[1]P. Campbell, I. Moore, and M. Pearson, "Laser spectroscopy for nuclear structure physics," Prog. Part. Nucl. Phys. **86**, 127–180 (2016).
[2]K. Chrysalidis, S. Wilkins, R. Heinke, A. Koszorus, R. De Groote, V. Fedosseev, B. Marsh, S. Rothe, R. G. Ruiz, D. Studer, A. Vernon, and K. Wendt, "First demonstration of Doppler-free 2-photon in-source laser spectroscopy at the ISOLDE-RILIS," Nucl. Instrum. Methods Phys. Res., Sect. B **463**, 476–481 (2020).
[3]J. Hu, A. Urvoy, Z. Vendeiro, V. Crépel, W. Chen, and V. Vuletić, "Creation of a Bose-condensed gas of $^{87}$Rb by laser cooling," Science **358**, 1078–1080 (2017).
[4]C. J. Baker, W. Bertsche, A. Capra, C. Carruth, C. L. Cesar, M. Charlton, A. Christensen, R. Collister, A. C. Mathad, S. Eriksson, A. Evans, N. Evetts, J. Fajans, T. Friesen, M. C. Fujiwara, D. R. Gill, P. Grandemange, P. Granum, J. S. Hangst, W. N. Hardy, M. E. Hayden, D. Hodgkinson, E. Hunter, C. A. Isaac, M. A. Johnson, J. M. Jones, S. A. Jones, S. Jonsell, A. Khramov, P. Knapp, L. Kurchaninov, N. Madsen, D. Maxwell, J. T. K. McKenna, S. Menary, J. M. Michan, T. Momose, P. S. Mullan, J. J. Munich, K. Olchanski, A. Olin, J. Peszka, A. Powell, P. Pusa, C. Ø. Rasmussen, F. Robicheaux, R. L. Sacramento, M. Sameed, E. Sarid, D. M. Silveira, D. M. Starko, C. So, G. Stutter, T. D. Tharp, A. Thibeault, R. I. Thompson, D. P. van der Werf, and J. S. Wurtele, "Laser cooling of antihydrogen atoms," Nature **592**, 35–42 (2021).
[5]M. Kues, C. Reimer, P. Roztocki, L. R. Cortés, S. Sciara, B. Wetzel, Y. Zhang, A. Cino, S. T. Chu, B. E. Little, D. J. Moss, L. Caspani, J. Azaña, and R. Morandotti, "On-chip generation of high-dimensional entangled quantum states and their coherent control," Nature **546**, 622–626 (2017).
[6]H.-H. Lu, J. M. Lukens, N. A. Peters, O. D. Odele, D. E. Leaird, A. M. Weiner, and P. Lougovski, "Electro-optic frequency beam splitters and tritters for high-fidelity photonic quantum information processing," Phys. Rev. Lett. **120**, 030502 (2018).
[7]K. K. Mehta, C. Zhang, M. Malinowski, T.-L. Nguyen, M. Stadler, and J. P. Home, "Integrated optical multi-ion quantum logic," Nature **586**, 533–537 (2020).
[8]J. M. Lukens and P. Lougovski, "Frequency-encoded photonic qubits for scalable quantum information processing," Optica **4**, 8–16 (2017).
[9]E. A. Kittlaus, N. T. Otterstrom, P. Kharel, S. Gertler, and P. T. Rakich, "Non-reciprocal interband Brillouin modulation," Nat. Photonics **12**, 613–619 (2018).
[10]D. B. Sohn, S. Kim, and G. Bahl, "Time-reversal symmetry breaking with acoustic pumping of nanophotonic circuits," Nat. Photonics **12**, 91–97 (2018).
[11]C. Joshi, A. Farsi, A. Dutt, B. Y. Kim, X. Ji, Y. Zhao, A. M. Bishop, M. Lipson, and A. L. Gaeta, "Frequency-domain quantum interference with correlated photons from an integrated microresonator," Phys. Rev. Lett. **124**, 143601 (2020).

[12]A. A. Savchenkov, W. Liang, A. B. Matsko, V. S. Ilchenko, D. Seidel, and L. Maleki, "Tunable optical single-sideband modulator with complete sideband suppression," Opt. Lett. **34**, 1300–1302 (2009).
[13]E. A. Kittlaus, W. M. Jones, P. T. Rakich, N. T. Otterstrom, R. E. Muller, and M. Rais-Zadeh, "Electrically driven acousto-optics and broadband non-reciprocity in silicon photonics," Nat. Photonics **15**, 43–52 (2021).
[14]K. Chrysalidis, V. N. Fedosseev, B. A. Marsh, R. P. Mildren, D. J. Spence, K. D. A. Wendt, S. G. Wilkins, and E. Granados, "Continuously tunable diamond Raman laser for resonance laser ionization," Opt. Lett. **44**, 3924–3927 (2019).
[15]E. Granados, D. J. Spence, and R. P. Mildren, "Deep ultraviolet diamond Raman laser," Opt. Express **19**, 10857–10863 (2011).
[16]D. T. Echarri, K. Chrysalidis, V. N. Fedosseev, B. A. Marsh, R. P. Mildren, S. M. Olaizola, D. J. Spence, S. G. Wilkins, and E. Granados, "Broadly tunable linewidth-invariant Raman Stokes comb for selective resonance photo-ionization," Opt. Express **28**, 8589–8600 (2020).
[17]Z. Bai, R. J. Williams, O. Kitzler, S. Sarang, D. J. Spence, Y. Wang, Z. Lu, and R. P. Mildren, "Diamond Brillouin laser in the visible," APL Photonics **5**, 031301 (2020).
[18]B. J. Eggleton, C. G. Poulton, P. T. Rakich, M. J. Steel, and G. Bahl, "Brillouin integrated photonics," Nat. Photonics **13**, 664–677 (2019).
[19]N. Chauhan, A. Isichenko, K. Liu, J. Wang, Q. Zhao, R. O. Behunin, P. T. Rakich, A. M. Jayich, C. Fertig, C. W. Hoyt, and D. J. Blumenthal, "Visible light photonic integrated Brillouin laser," Nat. Commun. **12**, 4685 (2021).
[20]O. Lux, S. Sarang, O. Kitzler, D. J. Spence, and R. P. Mildren, "Intrinsically stable high-power single longitudinal mode laser using spatial hole burning free gain," Optica **3**, 876–881 (2016).
[21]X. Yang, Z. Bai, D. Chen, W. Chen, Y. Feng, and R. P. Mildren, "Widely-tunable single-frequency diamond Raman laser," Opt. Express **29**, 29449–29457 (2021).
[22]S. Sarang, O. Kitzler, O. Lux, Z. Bai, R. J. Williams, D. J. Spence, and R. P. Mildren, "Single-longitudinal-mode diamond laser stabilization using polarization-dependent Raman gain," OSA Continuum **2**, 1028–1038 (2019).
[23]X. Yang, O. Kitzler, D. J. Spence, R. J. Williams, Z. Bai, S. Sarang, L. Zhang, Y. Feng, and R. P. Mildren, "Single-frequency 620 nm diamond laser at high power, stabilized via harmonic self-suppression and spatial-hole-burning-free gain," Opt. Lett. **44**, 839–842 (2019).
[24]O. Lux, S. Sarang, R. J. Williams, A. McKay, and R. P. Mildren, "Single longitudinal mode diamond raman laser in the eye-safe spectral region for water vapor detection," Opt. Express **24**, 27812–27820 (2016).
[25]E. Granados, C. Granados, R. Ahmed, K. Chrysalidis, V. N. Fedosseev, B. A. Marsh, S. G. Wilkins, R. P. Mildren, and D. J. Spence, "Spectral synthesis of multimode lasers to the Fourier limit in integrated Fabry–Perot diamond resonators," Optica **9**, 317–324 (2022).
[26]S. Rothe, B. A. Marsh, C. Mattolat, V. N. Fedosseev, and K. Wendt, "A complementary laser system for ISOLDE RILIS," J. Phys.: Conf. Ser. **312**, 052020 (2011).
[27]V. G. Savitski, S. Reilly, and A. J. Kemp, "Steady-state Raman gain in diamond as a function of pump wavelength," IEEE J. Quantum Electron. **49**, 218–223 (2013).
[28]T. Ruf, M. Cardona, C. S. J. Pickles, and R. Sussmann, "Temperature dependence of the refractive index of diamond up to 925K," Phys. Rev. B **62**, 16578–16581 (2000).
[29]G. Turri, S. Webster, Y. Chen, B. Wickham, A. Bennett, and M. Bass, "Index of refraction from the near-ultraviolet to the near-infrared from a single crystal microwave-assisted CVD diamond," Opt. Mater. Express **7**, 855–859 (2017).
[30]P. Jacobson and S. Stoupin, "Thermal expansion coefficient of diamond in a wide temperature range," Diamond Relat. Mater. **97**, 107469 (2019).
[31]M. S. Liu, L. A. Bursill, S. Prawer, and R. Beserman, "Temperature dependence of the first-order Raman phonon line of diamond," Phys. Rev. B **61**, 3391–3395 (2000).